

Unifying autocatalytic and zeroth-order branching models for growing actin networks

Julian Weichsel,^{1,2,*} Krzysztof Baczynski,¹ and Ulrich S. Schwarz^{1,†}

¹*Bioquant and Institute for Theoretical Physics, University of Heidelberg, Germany*

²*Department of Chemistry, University of California at Berkeley, United States*

(Received 17 July 2012; revised manuscript received 6 December 2012; published 3 April 2013)

The directed polymerization of actin networks is an essential element of many biological processes, including cell migration. Different theoretical models considering the interplay between the underlying processes of polymerization, capping, and branching have resulted in conflicting predictions. One of the main reasons for this discrepancy is the assumption of a branching reaction that is either first order (autocatalytic) or zeroth order in the number of existing filaments. Here we introduce a unifying framework from which the two established scenarios emerge as limiting cases for low and high filament numbers. A smooth transition between the two cases is found at intermediate conditions. We also derive a threshold for the capping rate above which autocatalytic growth is predicted at sufficiently low filament number. Below the threshold, zeroth-order characteristics are predicted to dominate the dynamics of the network for all accessible filament numbers. Together, these mechanisms allow cells to grow stable actin networks over a large range of different conditions.

DOI: [10.1103/PhysRevE.87.040701](https://doi.org/10.1103/PhysRevE.87.040701)

PACS number(s): 87.16.Ln, 87.10.-e, 87.15.R-, 87.17.Jj

In many situations of high biological relevance, including the migration of animal cells and the propulsion of specific intracellular pathogens, motility results from the directed polymerization of a dendritic actin filament network [1]. The organization of the growing network is determined mainly at the leading edge, where a small number of proteins regulate the interplay between three fundamental processes. The driving force for propulsion is polymerization of actin filaments from globular actin monomers. This is limited by capping proteins, which bind to the filament ends and prevent further polymerization. New filaments nucleate by branching off from mother filaments [2]. Although the biochemical details of this process are not yet completely understood, it is widely accepted that the branching complex Arp2/3 is activated by nucleation promoting factors (NPFs) such as WASP and SCAR/WAVE proteins [3,4]. When an activated Arp2/3 complex is bound to the side of an existing actin filament, a daughter filament starts to grow at a characteristic angle around 70° relative to the mother filament [compare Fig. 1(a)]. At the same time, the branch point moves away from the leading edge because of the ongoing polymerization of actin filaments.

Due to the high biological relevance and universal nature of the underlying processes, many theoretical models have been suggested to describe the characteristic features of growing actin networks [5]. However, in many cases contradictory predictions have been obtained, in particular regarding experimentally observed force-velocity relations [6–12] and the filament orientation distribution of the network [13–17]. Interestingly, many of these contradictions are a direct consequence of two different choices for the order of the branching reaction. In *autocatalytic models*, the branching rate is assumed to be proportional to the number of existing filaments in the network, i.e., it is modeled as a *first-order* reaction in filament density,

implicitly assuming an unlimited reservoir of activated Arp2/3 [13,18,19]. This yields growing actin networks for which a constant filament density is maintained only at a unique steady-state growth velocity. Increasing forces acting against the network reduce the speed of growth only transiently, as an increasing filament density subsequently lowers the force per filament back to the stationary level.

In marked contrast to the autocatalytic scenario, another class of models assumes that branching occurs with a constant rate, i.e., it is taken to be a *zeroth-order* reaction in filament density, corresponding to a limited supply of activated Arp2/3 [14,18,20]. Under these conditions, it has been shown that a continuum of steady-state velocities exists. Moreover, two competing steady-state filament orientation patterns are stable, namely, the ±35 and +70/0/−70 patterns shown schematically in Figs. 1(b) and 1(c), respectively. Transitions between these two fundamentally different network architectures can be triggered by changes in network growth velocity [13,20]. Indeed similar structural transitions have been demonstrated recently in electron microscopy data of the lamellipodium of keratocytes, indicating their physiological relevance [15,16]. In this Rapid Communication, we will show that the two contradictory model scenarios of autocatalytic and zeroth-order branching can be unified within a general theoretical framework that reconciles some of the seemingly contradictory observations and predictions.

Arp2/3 activation model. We first introduce a kinetic model for filament branching, based on a likely scenario for Arp2/3 activation [3,4,21]. Motivated by the dimensions of the lamellipodium for cells migrating on a flat substrate, we consider a two-dimensional situation in which the network slides away from the leading edge with a well-defined retrograde velocity v_{nw} . All reactions are assumed to occur in a small reaction zone extending from the leading edge over a nanometer-scale distance d_{br} . We consider a system of two variables: A is the concentration of Arp2/3 that is bound to the filaments but does not lead to a daughter branch yet. P is the concentration of NPFs which is available to activate bound Arp2/3 complexes to nucleate a daughter branch. The kinetic

*weichsel@berkeley.edu

†ulrich.schwarz@bioquant.uni-heidelberg.de

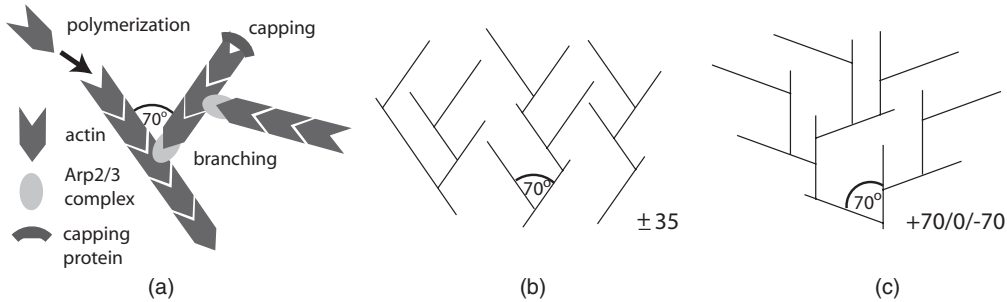


FIG. 1. (a) Interplay of polymerization, capping, and branching at the leading edge of an actin network growing towards the top. (b) A $\pm 35^\circ$ pattern is usually associated with dendritic actin networks. (c) However, theoretical and experimental evidence also exists for a $+70/0/-70^\circ$ pattern.

equations are

$$\begin{aligned} \frac{dA}{dt} &= k_+ N_{\text{fil}} - \left(k_- + \frac{v_{\text{nw}}}{d_{\text{br}}} \right) A - \tilde{k}_b A P, \\ \frac{dP}{dt} &= -\tilde{k}_b A P + k_{\text{act}}(P_0 - P). \end{aligned} \quad (1)$$

A increases as more complexes bind to the filaments with rate k_+ and decreases due to dissociation (rate k_-), outgrowth (rate $v_{\text{nw}}/d_{\text{br}}$), and branching (rate \tilde{k}_b). The last step also decreases available P , as NPFs that activate Arp2/3 are occupied for additional interactions with other Arp2/3 complexes at the same time until they become available again at rate k_{act} . P_0 is the total concentration of NPFs and N_{fil} is the number of actin filaments (because N_{fil} will be a central quantity of interest below, for our purpose it is convenient to consider the number of filaments in a reaction volume of finite lateral size rather than their concentration).

In steady state, Eq. (1) defines an effective rate of branching as $B^{\text{ss}} \equiv \tilde{k}_b A_{\text{ss}} P_{\text{ss}}$. This rate is a function of filament number N_{fil} as plotted in Fig. 2 for a typical set of parameters. At sufficiently small filament number N_{fil} , the effective branching

rate is approximately first order in N_{fil} and hence the coefficient of its linear expansion defines an autocatalytic branching rate constant k_b^{ac} :

$$B_0^{\text{ss}} = \frac{P_0 d_{\text{br}} k_+ \tilde{k}_b}{P_0 d_{\text{br}} \tilde{k}_b + d_{\text{br}} k_- + v_{\text{nw}}} N_{\text{fil}} \equiv k_b^{\text{ac}} N_{\text{fil}}. \quad (2)$$

In the limit of large filament number N_{fil} , B^{ss} saturates at a constant rate as assumed in zeroth-order branching models:

$$B_\infty^{\text{ss}} = P_0 k_{\text{act}}. \quad (3)$$

Thus the reaction smoothly changes from first to zeroth order as the filament number N_{fil} increases.

Actin growth model. We next analyze the effect of the order of the branching reaction on the steady growth states of actin networks. To this end, we extend a deterministic rate equation model that has been used before to describe both autocatalytic as well as zeroth-order branching actin networks [13,18,20]. The generic results reported here can be confirmed in computer simulations based on individual filaments and stochastic reactions [22]. We consider an ensemble of filaments located in the same reaction zone of width d_{br} as introduced above. Our central quantity is the distribution function $N(\theta, t)$ for the number of uncapped filaments orientated at time t at an angle θ with respect to the normal of the leading edge, which evolves in time as

$$\begin{aligned} \frac{dN(\theta, t)}{dt} &= -k_c N(\theta, t) - k_{\text{gr}}^\theta(v_{\text{nw}}) N(\theta, t) \\ &\quad + k_b \frac{\int_{-\pi}^{+\pi} \mathcal{W}(\theta, \theta') N(\theta', t) d\theta'}{\left(\int_{-\pi}^{+\pi} \int_{-\pi}^{+\pi} \mathcal{W}(\theta, \theta') N(\theta', t) d\theta' d\theta \right)^{1-\mu}}. \end{aligned} \quad (4)$$

Here the three terms on the right introduce capping, outgrowth from the reaction zone, and branching, respectively. While capping is simply a first-order process with constant rate, independent of filament orientation θ , for outgrowth we have to distinguish two cases. For $|\theta| \leq \arccos(v_{\text{nw}}/v_{\text{fil}})$, single filaments growing with velocity v_{fil} can keep up with the leading edge and thus $k_{\text{gr}}^\theta(v_{\text{nw}}) = 0$. If the orientation angle exceeds the threshold, filaments grow too slowly and leave the reaction region with rate $k_{\text{gr}}^\theta(v_{\text{nw}}) = (v_{\text{nw}} - v_{\text{fil}} \cos \theta)/d_{\text{br}}$.

In the branching term, $\mathcal{W}(\theta, \theta') = \mathcal{W}(|\theta - \theta'|)$ is a distribution function of the relative branching angle between mother and daughter filaments. Motivated by experimental observations, we approximate this function by the sum of two Gaussians centered around $\pm 70^\circ$ and each with standard

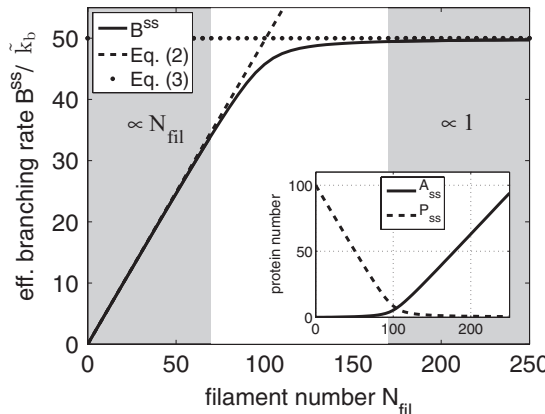


FIG. 2. Effective branching rate B^{ss} vs filament number N_{fil} in steady state. At low filament number the branching reaction is linear (autocatalytic) as given in Eq. (2) (dashed line), while at high filament number, a zeroth-order branching reaction is observed with a constant rate given by Eq. (3) (dotted line). The gray backgrounds mark the first- and zeroth-order regimes. The inset shows the corresponding steady-state concentrations of filament bound Arp2/3 (A_{ss} , solid line) and available NPFs (P_{ss} , dashed line).

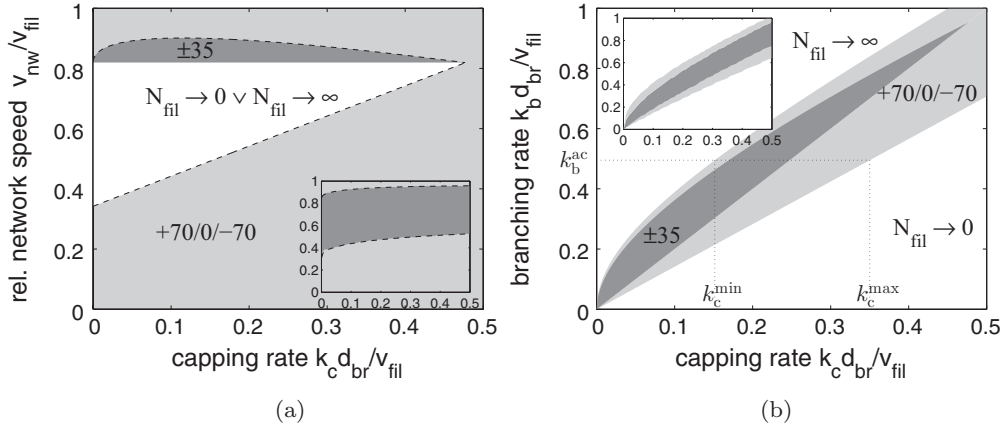


FIG. 3. Phase diagram predicted from linear stability analysis of the analytical model and by numerically solving the actin growth model [22]. (a) Projection onto (k_c, v_{nw}) plane. The dashed contour indicates identical transitions between $+70/0/-70$ and ± 35 patterns for all $0 \leq \mu \leq 1$. For $\mu = 1$, an additional constraint restricts the stable parameter space to the gray shaded regions. (b) Projection onto (k_c, k_b) plane for $\mu = 1$ (autocatalytic growth). Only a subset of the parameter values results in stable steady-state solutions.

deviation 5° . This corresponds well to the experimentally reported range of branching angles between 67° and 77° , which have been measured both using purified proteins [23,24] and in different cell lines [25,26]. The exact value of the branching angle, however, is irrelevant for our results.

The normalization of the branching term in Eq. (4) is appropriate to directly implement a specific reaction order μ in the actin growth model. In order to couple the actin growth model to the Arp2/3 activation model, below we will use numerical calculations with $\mu = 0$ and couple Eq. (1) and Eq. (4) via the filament number dependent branching rate $k_b(N_{fil}) = B^{ss}$ derived above, with $N_{fil} = \int N(\theta, t) d\theta$. For analytical progress and deeper insight, however, it is instructive to first analyze the steady states of the actin growth model with constant parameters k_b and μ . Indeed, it can be shown within the linear stability analysis employed below that both procedures are equivalent [22].

Steady-state analysis. The actin growth model Eq. (4) contains only four relevant parameters: the rates k_c and k_b for capping and branching, respectively, the network growth velocity v_{nw} , and the order of the branching reaction μ . By integrating the reaction model Eq. (4) over 35° sized angle bins and neglecting contributions from filaments growing in directions $>87.5^\circ$, we obtain three simplified coupled equations for the evolution of N_{0° , $N_{\pm 35^\circ}$ and $N_{\pm 70^\circ}$, which can be analyzed analytically. As an alternative which does not require any additional assumptions, we determine the stable regimes of network growth numerically, by propagating a finely discretized version of the equation until a steady state is reached.

In the analytical approach, there exist exactly two physically meaningful steady-state solutions, N^{ss70} and N^{ss35} , given by

$$\begin{aligned} N_{0^\circ}^{ss70} &= \frac{-k_c - k_{gr}^{70^\circ} + \sqrt{2k_c(k_c + k_{gr}^{70^\circ})}}{k_c - k_{gr}^{70^\circ}} C_1^{1/(1-\mu)}, \\ N_{\pm 35^\circ}^{ss} &= 0, \\ N_{\pm 70^\circ}^{ss70} &= \frac{2k_c - \sqrt{2k_c(k_c + k_{gr}^{70^\circ})}}{k_c - k_{gr}^{70^\circ}} C_1^{1/(1-\mu)}, \end{aligned} \quad (5)$$

and

$$N_{0^\circ}^{ss35} = N_{\pm 70^\circ}^{ss35} = 0, \quad N_{\pm 35^\circ}^{ss35} = C_2^{1/(1-\mu)}, \quad (6)$$

where

$$C_1 = k_b / \sqrt{2k_c(k_c + k_{gr}^{70^\circ})}, \quad C_2 = k_b / (2k_c + 2k_{gr}^{35^\circ}). \quad (7)$$

These two fixed points correspond to the two competing orientation patterns depicted schematically in Figs. 1(c) and 1(b), respectively. Linear stability analysis shows that for $\mu > 1$, both are saddle points and thus no stable solution exists. In contrast, $\mu \leq 1$ leads to mutually exclusive stability of the two solutions [22]. Figure 3(a) shows the regions of stability for each of the two orientation patterns within the two-dimensional parameter space spanned by k_c and v_{nw} . The dashed contour indicates transitions between a $+70/0/-70$ pattern outside and a ± 35 pattern inside. Remarkably, the transition is independent of k_b and μ and thus all cases with $\mu \leq 1$ show no difference in the locations of the transitions. The result from the full numerical analysis of Eq. (4) is shown as an inset. The main difference between the analytical and numerical results is that the stability of the ± 35 pattern vanishes for large k_c in the analytical model, because it disregards contributions from filament orientations $\gtrsim 90^\circ$. This increases the stability of the $+70/0/-70$ pattern, when outgrowth of filaments is negligible compared to capping.

Until now we have shown that for all reaction orders of interest ($0 \leq \mu \leq 1$), two orientation patterns compete for stability, with phase boundaries being independent of the exact value of μ . Nevertheless the limit $\mu \rightarrow 1$ (autocatalytic growth) is special, because in this case, finite steady-state solutions only exist if additional constraints are satisfied. Due to Eq. (5), N^{ss70} is finite only when $C_1 = 1$. From Eq. (7) this requires $k_{gr}^{70^\circ}(v_{nw})k_c + k_c^2 = k_b^2/2$. Due to Eq. (6), N^{ss35} is finite only when $C_2 = 1$. From Eq. (7) this requires $k_{gr}^{35^\circ}(v_{nw}) + k_c = k_b/2$. Therefore, if a stable steady-state solution exists for given values of k_c and k_b , then for $\mu = 1$ it corresponds to a unique network growth velocity v_{nw} . In this way, the most prominent feature of autocatalytic growth [18] emerges in our unifying model. Due to these additional conditions, stable solutions are

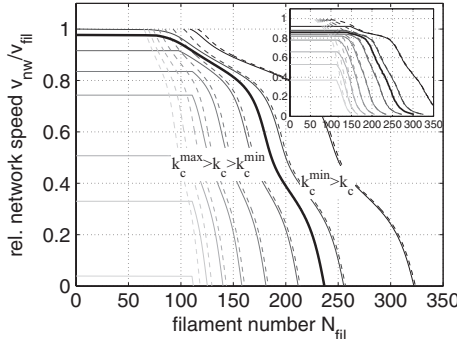


FIG. 4. Network growth velocity as a function of filament number for different capping rates k_c as obtained numerically from the unified model (solid lines). Darker gray indicates decreasing k_c . The dashed lines show the results from a zeroth-order description. For capping rates $k_c^{\min} \lesssim k_c \lesssim k_c^{\max}$, an autocatalytic regime is observed at low filament density. The capping rate $k_c = k_c^{\min}$ (thick black solid line) marks the transition to pure zeroth-order behavior. The inset shows the results from stochastic computer simulations.

restricted in parameter space to a lower dimensional manifold, which in case of the analytical model has a jump discontinuity [22]. In Fig. 3(a) we show the projection of this manifold onto the (k_c, v_{nw}) plane with bright and dark gray regions marking the stability regions for the $+70/0/-70$ and ± 35 patterns, respectively. As the inset indicates, a jump discontinuity is not observed in the full numerical treatment.

In Fig. 3(b), the manifold for $\mu = 1$ is projected onto the (k_c, k_b) plane (in this projection, the jump discontinuity cannot be seen). Only a subset of (k_b, k_c) combinations yields stable autocatalytic growth with finite filament number N_{fil} . This important result is predicted both by the analytical and the numerical approach (compare inset).

Limits of autocatalytic network growth. Using the insights obtained in the preceding sections from the actin growth model Eq. (4) with μ as a model parameter, we now combine the Arp2/3 activation model Eq. (1) and the actin growth model Eq. (4) with $\mu = 0$ to arrive at a unifying theoretical framework for actin network growth with a branching reaction that is determined by a regulatory process. Figure 4 shows our numerical results for network growth velocity v_{nw} as a function of filament number N_{fil} (solid lines) for various values of the capping rate k_c . They agree very well with the results from stochastic computer simulations shown as an inset [22]. At sufficiently low filament number, we observe an autocatalytic regime where a whole range of values for N_{fil} corresponds to the same velocity. For larger N_{fil} , however, the steady-state network velocity starts to decrease similarly to a pure zeroth-order description (dashed lines). These changes include transitions between the two dominant filament orientation patterns as predicted in Fig. 3.

Interestingly, the details of the crossover from first- to zeroth-order branching strongly depend on the capping rate. This can be understood in the analytical model analyzed above. At low filament density, branching is effectively a first-order reaction and thus the conditions $C_1 = 1$ and $C_2 = 1$, previously derived from Eqs. (5)–(7) for $\mu = 1$, need to be satisfied here for stable growth as well. By inserting the autocatalytic branching rate k_b^{ac} defined in Eq. (2) into

Eq. (7) and applying the relevant first-order condition, we are able to derive estimates for minimum and maximum capping rates k_c^{\min} and k_c^{\max} corresponding to the largest and smallest possible network velocities, $v_{\text{nw}}/v_{\text{fil}} = 1$ and $v_{\text{nw}}/v_{\text{fil}} = 0$, respectively:

$$k_c^{\min} = \frac{v_{\text{fil}}}{2d_{\text{br}}} \left[c + \sqrt{2 \left(\frac{k_b^{\text{ac}} d_{\text{br}}}{v_{\text{fil}}} \right)^2 + c^2} \right], \quad k_c^{\max} = \frac{k_b^{\text{ac}}}{\sqrt{2}}, \quad (8)$$

where $c = \cos 70^\circ - 1$. These two threshold values are shown in Fig. 3(b) as the intersection of k_b^{ac} with the boundaries of the stable autocatalytic parameter subset. Comparison of Eq. (8) with the numerical results from the full model presented in Fig. 4 shows that our analytical approach captures the location of this crossover very well and thus accurately explains the observed behavior. For increasing k_c , the network velocity in the autocatalytic region decreases until at around $k_c \simeq k_c^{\max}$ the filament number decays to zero for all accessible network velocities. For decreasing k_c , the network growth velocity reaches its maximal value at $k_c \lesssim k_c^{\min}$ (thick solid line), when the network is not able to balance filament branching by capping and outgrowth anymore. In a purely autocatalytic model, this would lead to a diverging and therefore unphysical filament number. Within our unifying framework, the number of filaments increases only to the point where zeroth-order growth behavior starts to dominate and stabilizes a steady state at finite filament number. In this regime, the results from the full model (solid) agree with a zeroth-order branching model (dashed).

Relation to experiments. In this Rapid Communication, we have developed a theoretical framework that reconciles conflicting results from two classes of actin growth models and explains many experimental observation: an autocatalytic growth regime at low filament density [6,9], zeroth-order characteristics at high density [7,8], network velocity-dependent transitions in filament orientation patterns [15,16], and bistability and hysteresis at these transitions [9,20]. Strikingly our model naturally avoids the instability which occurs at low capping rate in the autocatalytic model.

Our model also makes testable predictions that can guide future experiments. Using single-molecule microscopy either in migrating cells [27] or in reconstituted assays, the number of branching events can be directly correlated to filament density, which can be compared to the effective branching rate as predicted in Fig. 2. From electron microscopy data, filament orientations can be extracted and correlated with the growth velocity as demonstrated in [15,16]. This can be compared to the unified phase diagram in Fig. 3. Finally, reconstituted actin networks growing against a functionalized cantilever of an atomic force microscope (AFM) or bead [8,9,28] are predicted to yield an autocatalytic (i.e., force-insensitive) growth velocity for sufficiently low load and high concentration of capping protein. In this regime the filament density near the obstacle is thus expected to grow proportionally to the applied force. When either the concentration of capping protein is reduced below the threshold k_c^{\min} [Eq. (8)] or the load on the network is sufficiently increased, zeroth-order behavior is predicted to take over as illustrated in Fig. 4.

Acknowledgments. J.W. was supported by the research unit for systems biology ViroQuant at Heidelberg and by the Deutsche Forschungsgemeinschaft (DFG) at Berkeley (Grant

No. We 5004/2-1). U.S.S. acknowledges support as a member of the cluster of excellence CellNetworks at Heidelberg University.

-
- [1] *Actin-based Motility*, edited by M. F. Carlier (Springer, Houten, Netherlands, 2010).
 - [2] T. D. Pollard, *Annu. Rev. Biophys. Biomol. Struct.* **36**, 451 (2007).
 - [3] C. C. Beltzner and T. D. Pollard, *J. Biol. Chem.* **283**, 7135 (2008).
 - [4] X. P. Xu, I. Rouiller, B. D. Slaughter, C. Egile, E. Kim, J. R. Unruh, X. Fan, T. D. Pollard, R. Li, D. Hanein *et al.*, *EMBO J.* **31**, 236 (2012).
 - [5] A. Mogilner, *J. Math. Biol.* **58**, 105 (2009).
 - [6] S. Wiesner, E. Helfer, D. Didry, G. Ducouret, F. Lafuma, M. F. Carlier, and D. Pantaloni, *J. Cell Biol.* **160**, 387 (2003).
 - [7] J. L. McGrath, N. J. Eungdamrong, C. I. Fisher, F. Peng, L. Mahadevan, T. J. Mitchison, and S. C. Kuo, *Curr. Biol.* **13**, 329 (2003).
 - [8] Y. Marcy, J. Prost, M. F. Carlier, and C. Sykes, *Proc. Natl. Acad. Sci. USA* **101**, 5992 (2004).
 - [9] S. H. Parekh, O. Chaudhuri, J. A. Theriot, and D. A. Fletcher, *Nat. Cell Biol.* **7**, 1219 (2005).
 - [10] M. Prass, K. Jacobson, A. Mogilner, and M. Radmacher, *J. Cell Biol.* **174**, 767 (2006).
 - [11] F. Heinemann, H. Doschke, and M. Radmacher, *Biophys. J.* **100**, 1420 (2011).
 - [12] J. Zimmermann, C. Brunner, M. Enculescu, M. Goegler, A. Ehrlicher, J. Käs, and M. Falcke, *Biophys. J.* **102**, 287 (2012).
 - [13] I. V. Maly and G. G. Borisy, *Proc. Natl. Acad. Sci. USA* **98**, 11324 (2001).
 - [14] S. Schaub, J. J. Meister, and A. B. Verkhovsky, *J. Cell Sci.* **120**, 1491 (2007).
 - [15] S. A. Koestler, S. Auinger, M. Vinzenz, K. Rottner, and J. V. Small, *Nat. Cell Biology* **10**, 306 (2008).
 - [16] J. Weichsel, E. Urban, J. V. Small, and U. S. Schwarz, *Cytometry Part A* **81A**, 496 (2012).
 - [17] A. B. Verkhovsky, O. Y. Chaga, S. Schaub, T. M. Svitkina, J. J. Meister, and G. G. Borisy, *Mol. Biol. Cell* **14**, 4667 (2003).
 - [18] A. E. Carlsson, *Biophys. J.* **84**, 2907 (2003).
 - [19] T. E. Schaus, E. W. Taylor, and G. G. Borisy, *Proc. Natl. Acad. Sci. USA* **104**, 7086 (2007).
 - [20] J. Weichsel and U. S. Schwarz, *Proc. Natl. Acad. Sci. USA* **107**, 6304 (2010).
 - [21] S.-C. Ti, C. T. Jurgenson, B. J. Nolen, and T. D. Pollard, *Proc. Natl. Acad. Sci. USA* **108**, E463 (2011).
 - [22] See Supplemental Material at <http://link.aps.org/supplemental/10.1103/PhysRevE.87.040701> for more details.
 - [23] R. D. Mullins, J. A. Heuser, and T. D. Pollard, *Proc. Natl. Acad. Sci. USA* **95**, 6181 (1998).
 - [24] L. Blanchoin, K. J. Amann, H. N. Higgs, J. B. Marchand, D. A. Kaiser, and T. D. Pollard, *Nature* **404**, 1007 (2000).
 - [25] T. M. Svitkina and G. G. Borisy, *J. Cell Biol.* **145**, 1009 (1999).
 - [26] M. Vinzenz, M. Nemethova, F. Schur, J. Mueller, A. Narita, E. Urban, C. Winkler, C. Schmeiser, S. Koestler, K. Rottner *et al.*, *J. Cell Sci.* **125**, 2775 (2012).
 - [27] A. Millius, N. Watanabe, and O. D. Weiner, *J. Cell Sci.* **125**, 1165 (2012).
 - [28] O. Chaudhuri, S. H. Parekh, W. A. Lam, and D. A. Fletcher, *Nat. Methods* **6**, 383 (2009).